Corneal Potential Maps Measured With Multi-Electrode Electroretinography in Rat Eyes With Experimental Lesions

Zahra Derafshi,[1] Brian E. Kunzer,[1] Emily M. Mugler,[2] Nataliya Rokhmanova,[1] Dong-Wook Park,[3] Hadi Tajalli,[1] Krithi Shetty,[1] Zhenqiang Ma,[3] Justin C. Williams,[4] and John R. Hetling[1]

[1]Department of Bioengineering, University of Illinois at Chicago, Chicago, Illinois, United States
[2]Northwestern University, Department of Neurology, Chicago, Illinois, United States
[3]Department of Electrical and Computer Engineering, University of Wisconsin-Madison, Madison, Wisconsin, United States
[4]Department of Biomedical Engineering, University of Wisconsin-Madison, Madison, Wisconsin, United States

Correspondence: John R. Hetling, Department of Bioengineering, University of Illinois at Chicago, 851 S. Morgan Street, SEO 232, MC 063, Chicago, IL 60607, USA; JHetli1@uic.edu.

Submitted: September 9, 2016
Accepted: April 2, 2017

Citation: Derafshi Z, Kunzer BE, Mugler EM, et al. Corneal potential maps measured with multi-electrode electroretinography in rat eyes with experimental lesions. *Invest Ophthalmol Vis Sci*. 2017;58:2863–2873. DOI:10.1167/iovs.16-20726

Purpose. Conventional full-field flash electroretinography (ERG) yields a single response waveform that can be useful in the early detection and diagnosis of many diseases affecting the retina. It is an objective measurement that probes the entire retina. However, localized areas of dysfunction have relatively small influence on ERG amplitudes compared to normal ranges. Here we evaluate the use of corneal potential maps obtained in response to full-field flash stimuli for sensitivity to local areas of retinal damage.

Methods. A contact lens electrode array was used to record 25 ERG waveforms simultaneously following saturating full-field flash stimuli (multi-electrode electroretinography, meERG) in rats. Waveforms were evaluated for a-wave and b-wave amplitudes; these values were normalized and further evaluated for spatial differences across the corneal surface. Cluster analysis and a support vector machine approach were used to classify meERG responses from healthy eyes and eyes with central (photocoagulation) or peripheral (cryocoagulation) experimental lesions.

Results. A normative normalized corneal potential map was obtained from healthy eyes ($n = 26$). Corneal potential maps from eyes with experimental lesions ($n = 13$) could be classified with sensitivity and specificity of approximately 80% based solely on the normalized spatial distribution of corneal potentials, that is, with no knowledge of absolute amplitudes.

Conclusions. Corneal potential maps obtained in response to full-field flash stimuli are altered in eyes with scotomas in the central and far-peripheral retina. The meERG approach yields useful spatial information following a single brief flash, analogous to body-surface potential maps used to evaluate heart and brain.

Keywords: corneal potential map, contact lens electrode array, multi-electrode electroretinography, peripheral retina, flash electroretinography

Many diseases that affect the retina begin with localized areas of dysfunction that then spread to ever increasing areas unless effectively managed. Among the most prevalent eye diseases, the earliest damage can present in the central, middle, or peripheral retina (e.g., macular degeneration, glaucoma, retinitis pigmentosa, respectively). The strong correlation between earlier management and favorable patient outcomes motivates the development of objective functional tests that are sensitive to local areas of retinal dysfunction and that are practical in a clinical setting (e.g., placing a reasonable burden on the patient to achieve informative results).

Electroretinography (ERG) can provide a high level of detail regarding retinal function. With the appropriate choice of stimulus, recording protocol, and analysis, it is possible to probe the response of specific classes of cells and functional pathways. Full-field flash ERG is relatively simple to perform yet lacks sensitivity to small areas of local dysfunction. The conventional flash ERG response is the averaged contribution from the entire retina; a scotoma that spans 5% of the area of the retina could be expected to reduce the ERG amplitude by approximately 5% (more or less depending on the eccentricity of the scotoma and local cell density). However, normative ranges for conventional flash ERG protocols are several times this expected effect size, for example, from 35% below to 72% above the median value for maximum dark adapted a-wave amplitudes,[1] resulting in very low sensitivity to modest localized damage.

The multi-focal ERG (mfERG) provides excellent sensitivity to localized dysfunction within the area probed by the stimulus, typically the central 20° to 25° of visual angle.[2,3] However, mfERG requires good acuity, can be arduous for some patients because of the requirement for extended fixation times, and is difficult to apply to the peripheral retina or to the rod pathway.

The motivation for multi-electrode ERG (meERG) is to increase sensitivity to localized dysfunction compared to

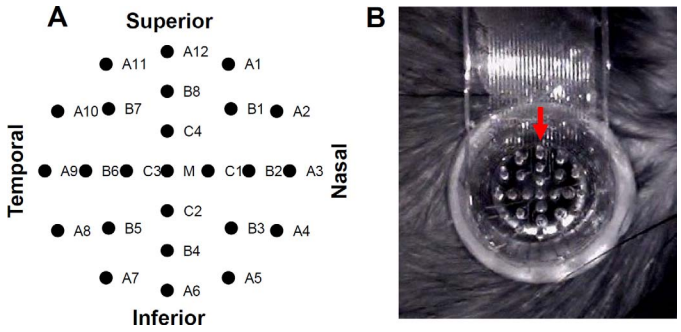

Figure 1. Electrode positions of the Contact Lens Electrode Array (CLEAr Lens). (**A**) The 25 electrodes are arranged in three concentric rings (A, B, and C) plus a central electrode (M). Electrode A12 is always at the superior margin of the cornea. All responses presented here were obtained from right eyes; electrode A3 is always at the nasal margin of the cornea. (**B**) Photograph taken with an infrared camera during an experiment; lens position is monitored throughout the recording. Electrode A12 is indicated by a *red arrow*.

conventional single electrode ERG while retaining the advantages of full-field flash ERG (no stringent requirements for fixation or acuity, short test duration, evaluates entire visual field, several established protocols available to probe many aspects of retinal function). That local retinal lesions alter the distribution of ocular surface potentials has been known for decades,[4,5] although these earlier efforts used either two pairs of differential scleral electrodes or a single electrode moved from location to location on the eye surface. Previously we presented a method to record meERG potentials at 25 locations on the cornea simultaneously,[6] allowing more comprehensive measurement and analysis of spatial differences in corneal potentials.

Here we report an initial evaluation of meERG sensitivity and specificity to local experimental lesions in rat eyes. Corneal potential maps were recorded with a contact lens electrode array and analyzed for changes in the spatial distribution of corneal potentials associated with the local lesions. These data will support validation of bioelectric models that relate local retinal activity to corneal potentials, which can then be used to predict the retinal source distribution (i.e., a functional map of the retina) from the response to a single full-field flash.[7,8] This approach is analogous to functional heart and brain mapping based on body surface potential maps.[9,10]

Methods

Recording Electrode

meERG responses were recorded with a 25-channel contact lens electrode array (CLEAr Lens) sized for rat eyes; the CLEAr Lens design, properties, and basic recording protocol have been described previously.[6] The 25 electrodes are arranged in three concentric rings (A, B, C) plus one central electrode (M), as shown in Figure 1. The A ring electrodes made contact with the cornea near the limbus, and electrode A12 was always located in the superior position, A3 in the nasal position (all responses in this report are from right eyes).

Experimental Design

Rats were purchased in small cohorts of two to four animals. After 2 days of acclimation, meERG responses were obtained from the right eye of each animal (pretreatment meERG). At 2 to 3 days after the first meERG recording, one half of each cohort (lesion group) received an experimental lesion to the retina in the right eye; the other half of the cohort served as the control group (underwent the same anesthesia but received no lesion). At 2 to 3 days after the lesions were created, a second set of responses was obtained from the right eye of all animals in the cohort (posttreatment meERG). All pretreatment responses, and the posttreatment responses from the control group, were considered normal eye responses for analysis. The left eyes were not used as controls because of the extensive effort required to reconfigure the meERG system between right- and left-eye recording.

Animals

Long Evans rats (Charles River, Wilmington, MA, USA) were obtained in the age range of 6 to 7 weeks, when the radius of curvature of the cornea matches the base curve of the CLEAr Lens. For all experimental procedures, the cornea was anesthetized with 0.5% proparacaine, and the pupils were dilated with 2.5% phenylephrine hydrochloride and 1% tropicamide. Prior to meERG recording, the animals were dark adapted for at least 1 hour; general anesthesia was obtained by intraperitoneal injection of ketamine and xylazine (100 and 10 mg [kg body weight]$^{-1}$, respectively). A regulated heating pad was used to maintain animals at 37°C to 39°C during meERG recording. Following the posttreatment recording session, fluorescein dye was used to examine the cornea for abrasion. During the treatment session, the animals were anesthetized by intraperitoneal injection of ketamine and acepromazine (100 and 5 mg [kg body weight]$^{-1}$, respectively). Animals receiving lesions also received a sub-Q injection of meloxicam (1 mg [kg body weight]$^{-1}$; Loxicom, 5 mg/mL; Norbrook Laboratories Limited, Newry County Down, Northern Ireland) for analgesia. All experiments were performed in accordance with the ARVO Statement for the Use of Animals in Ophthalmic and Visual Research.

Central Retina Lesions

Localized lesions in the central retina were created using laser photocoagulation. A 532 nm diode-pumped solid-state laser (model LRS-0532-PF; Laserglow Technologies, Toronto, ON, Canada) was focused through one path of a stereomicroscope (Nikon SMZ1000; Nikon Instruments, Inc., Melville, NY, USA) to a spot size of approximately 250 μm at the retina. Energy of 8.15e-3 μJ/μm^2 per pulse was delivered, representing the average value in four reported protocols (range, 1.36e-3 to 1.52e-2 μJ/μm^2).[11–14] Clusters of nonoverlapping burns were created to cover an area of 0.94 to 2.29 mm^2 (~3% of retinal area). Lesions were created near the optic nerve head (ONH), but restricted to one hemisphere. The location of the lesion was selected to avoid major blood vessels on the vitreal surface

Investigative Ophthalmology & Visual Science

of the retina. Fundus photographs of the retina were taken immediately after treatment.

Peripheral Retina Lesions

Because the photocoagulation laser could not be focused on the far-peripheral retina, localized lesions in the peripheral retina were created using cryocoagulation. A cryocoagulation probe with a tip diameter of 2.0 mm was custom machined from brass. The probe was submerged in liquid nitrogen for at least 20 minutes prior to use. The tip of the probe was applied to the scleral surface just posterior to the limbus with gentle pressure for 26 seconds. The probe was then removed, and the area of damage confirmed by viewing the peripheral retina through a plano-concave lens and ophthalmic surgical microscope (area of retina beneath probe tip location appeared white). The retina and RPE experienced permanent damage, whereas the sclera and choroid appeared to recover.[15]

meERG Recording

Following CLEAr Lens placement under dim red light, the lens was allowed to settle for 5 to 10 minutes, which also allowed for the body temperature to stabilize. CLEAr Lens electrodes were referenced to a platinum subdermal needle electrode in the nape of the neck; a second needle electrode in the back served as ground. Full-field flash stimuli were delivered via an acrylic dome back-lit by a Xenon flash lamp (Model 2100C, Novatron of Dallas, Inc., Dallas, TX, USA). A bright flash of 1033 scotopic candela seconds per meter squared (sc cd s m^{-2}; duration <100 μS) was used to ensure that all areas of the retina were responding at or near saturation levels even if the retinal illuminance was not perfectly uniform because of the presence of the CLEAr Lens. Following each flash, up to 25 meERG waveforms were simultaneously recorded (see Fig. 2A), passband 0.2 to 500 Hz, sampling rate 5 kHz. Interflash intervals of 90 seconds allowed the retina to recover between stimuli. Before and after every experiment, a sine wave (1 mV peak-to-peak, 200 Hz) was delivered to the CLEAr Lens to assess channel viability. Stimulus delivery and data recording were managed by MCRack software (Multi-Channel Systems MCS GmbH, Reutlingen, Germany).

Imaging and Histology

In six animals, optical coherence tomography (OCT) images of the damaged area of the retina were obtained within 1 hour of the posttreatment meERG recording session (Heidelberg Spectralis, Heidelberg Engineering, Inc., Franklin, MA, USA) to assess acute effects of the photocoagultion and cryocoagulation procedures that might be obscured by tissue processing for histology. Immediately following the posttreatment meERG recording (or OCT imaging), each animal was killed via CO_2 asphyxiation, the superior cornea marked with a cautery burn, the right eye removed, and the cornea slit with a razor blade. Fixative (2% paraformaldehyde, 2.5% glutaraldehyde) was injected into the vitreal cavity through the corneal slit, and the eye was immersed in fixative for 2 to 7 days, followed by immersion in alcohol for storage until histologic processing. Following fixation, but prior to histologic sectioning, the cornea was dissected away and four slits were cut extending from the limbal region toward the posterior pole to create a flat-mount eye cup for photographic documentation of lesion area and location. Lesion areas were outlined manually and the area calculated using ImageJ software (http://imagej.nih.gov/ij/; provided in the public domain by the National Institutes of Health, Bethesda, MD, USA). The tissue was then processed for

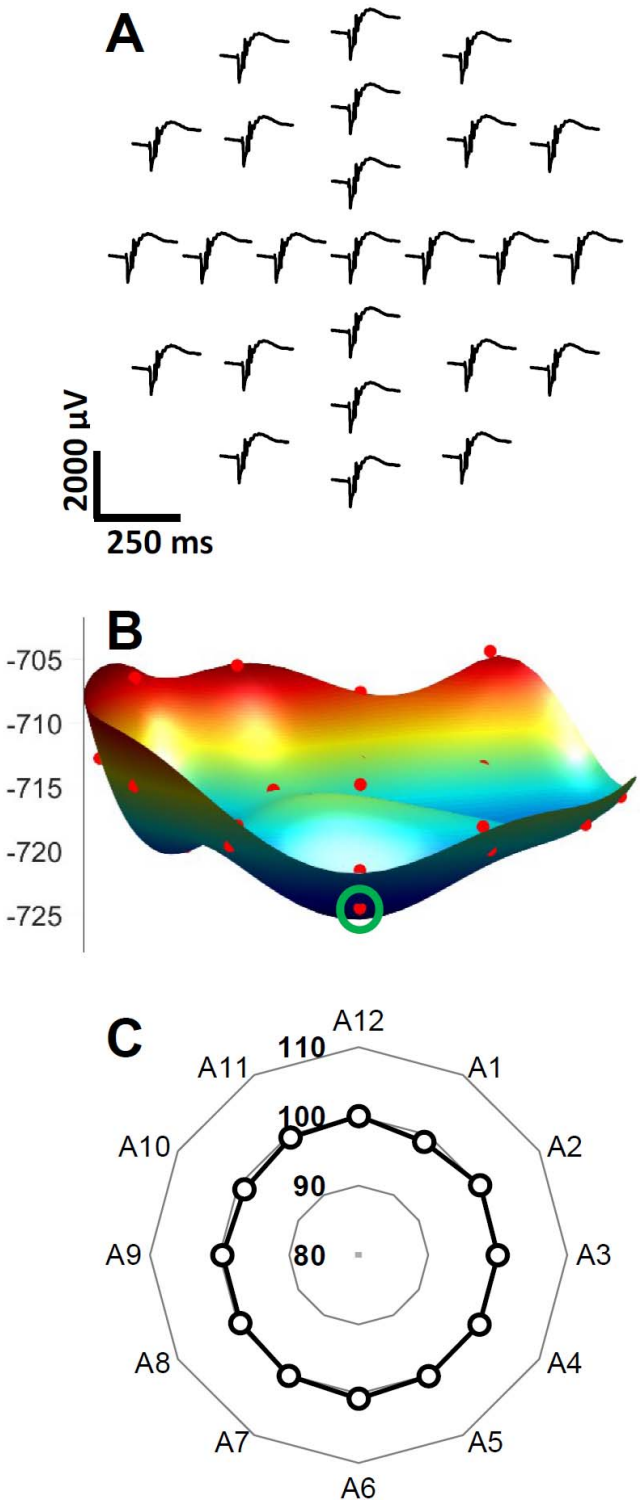

Figure 2. Representative meERG response from a normal (i.e., no experimental damage) eye. (**A**) A total of 25 meERG waveforms were recorded simultaneously after presenting a single bright flash (1033 sc cd s m^{-2}); waveforms plotted in the relative positions from which they were recorded on the cornea. (**B**) Potential map of the cornea obtained by interpolating between the 25 measured potentials (electrode locations indicated by *red dots*) at $t = 4$ ms (leading edge of a-wave) using a three-dimensional spline (Equation 1); amplitude is double coded as height and color for visual clarity, scale is in μV. The potential map is rotated so that the superior retina is in the foreground, electrode A12 is circled in *green*. (**C**) Amplitude of each A ring electrode (A1–A12) normalized to the mean amplitude recorded on the central five electrodes (C1-C4, M; Equation 3), presented as a "radar plot" to visualize spatial asymmetry in corneal potentials.

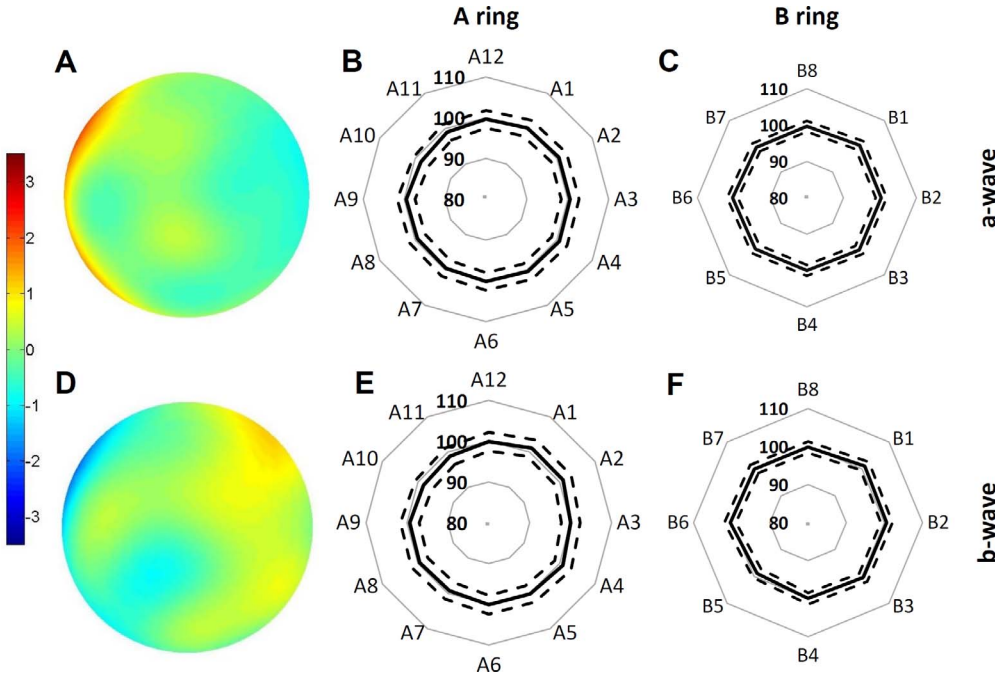

Figure 3. Normative data set ($n = 26$). (**A**) Average corneal potential map evaluated at $t = 4$ ms (leading edge of a-wave), obtained after converting each individual potential map to standard scores (Equation 2). Color scale is in units of standard deviations from the spatial mean. (**B**) Average ratio values for A ring electrodes evaluated at $t = 4$ ms; *dashed lines* plot ± 2 SD. (**C**) Average ratio values for B ring electrodes evaluated at $t = 4$ ms; *dashed lines* plot ± 2 SD. (**D–F**) Average corneal potentials evaluated at the peak of the b-wave; analysis as in **A** through **C**.

histology to verify the extent of cellular damage (thin sections through lesion area, hematoxylin and eosin stain).

Analysis

Criteria were set to ensure that data included in the analysis were of high quality. Individual recording channels on a CLEAr Lens were disregarded if the sine wave testing (see earlier) indicated excessive noise before or after the experiment or if recorded waveform amplitudes were more than 1.5× above or below the mean amplitude on the other channels. Individual meERG responses (25 channel response following a flash stimulus) were disregarded if contaminated by obvious artifacts. Individual recording sessions (all data collected on a given day from an individual animal) were disregarded if more than five channels were not producing clean response waveforms or if three or more neighboring channels in any one ring were not producing clean response waveforms or for normal eye responses if the standard deviation of the A ring amplitude ratios (described in Equation 3) was greater than 11. The criterion level of 11 resulted in inclusion of the most informative data sets (i.e., yielded highest area under the receiver-operator characteristic [ROC] curves) when compared with other criterion levels between 5 and 20. The numbers of data sets included in the full analysis were 26 from normal eyes (pretreatment in both groups plus posttreatment in control group, of 39 recorded), 4 eyes with central lesions (of five recorded), and 9 eyes with peripheral lesions (of 11 recorded).

Corneal Potential Maps

The first analysis step was to interpolate corneal potential values between the electrode locations, which formed smooth corneal potential color maps for visualization, and filled in for missing channels prior to further analysis (see Fig. 2B). This was accomplished by adapting a three-dimensional spline approach developed to interpolate electroencephalography data,[16] Equation 1.

$$\varphi(x,y,z) = \sum_{i=1}^{n} p_i K_{m-1}(x - x_i, y - y_i, z - z_i) + \sum_{d=0}^{m-1}\sum_{k=0}^{d}\sum_{g=0}^{k} q_{dkg} x^{d-k} y^{k-g} z^{g} \quad (1)$$

where,

$$K_{m-1}(s,t,r) = (s^2 + t^2 + r^2)^{m-1} \log(s^2 + t^2 + r^2 + w^2)$$

$$s = x - x_i \qquad t = y - y_i \qquad r = z - z_i$$

In Equation 1, φ is the interpolated potential at the point (x, y, z), which represent 3,796 points on the corneal surface, which is assumed to have a spherical profile during recording (while conforming to the concave surface of the CLEAr Lens). x_i, y_i, z_i is the location of electrode i, n is the number of electrodes (25), and w is the diameter of the electrode. Variable p_i is the coefficient of the basis function, q_{dkg} is the coefficient of the osculating function, and m is the parameter that controls the order of spline, given a value of 3 based on the work of Law et al.[16] The coefficients p and q are initially solved by inserting the electrode positions and potentials on those electrodes.

To compare the spatial differences in corneal potentials across animals, the measured and interpolated values were converted to standard score (s_i, number of standard deviations from the mean) using Equation 2.

$$s_i = \frac{V_i - \bar{V}_{measured}}{\sigma_{measured}} \quad (2)$$

In Equation 2, V_i is the potential at each location i, $\bar{V}_{measured}$ is

the average of the measured potentials, and $\sigma_{measured}$ is the standard deviation of the measured potentials. Although ERG amplitudes across populations are not normally distributed, the meERG potentials across the cornea are well described by a normal distribution (not shown).

Quantifying Spatial Asymmetry

The unique information provided by meERG recording is the spatial differences in corneal potentials. The main hypothesis of this study is that the spatial distribution of these potentials is altered when an experimental scotoma is present. To quantify the spatial distribution of potentials, the ratios between peripheral and central corneal locations were calculated.[6] Ratios are often used in ERG analysis to minimize effects of repeated-measure and intersubject variance in absolute amplitudes. The measured amplitude on each of the 12 peripheral electrodes in the A ring, or the 8 electrodes in the B ring (Fig. 1), were divided by the average amplitude measured on the central five electrodes (C ring plus M) and multiplied by 100, as given in Equation 3.

$$R_i = \frac{V_i \times 100}{(V_{C1} + V_{C2} + V_{C3} + V_{C4} + V_M)/5} \quad (3)$$

where i is the electrode number (c.f. Fig. 1), which ranged from 1 to 12 for A ring ratios and from 1 to 8 for B ring ratios. These ratios were plotted by electrode position for both A ring and B ring separately as "radar plots." These radar plots were produced for both a-wave and b-wave amplitudes. An example radar plot for a-wave amplitudes of one animal is shown in Figure 2C.

Lesion Detection

A cluster analysis was performed to assess whether the spatial distribution of corneal potentials could be used to identify eyes with experimental lesions. The amplitude ratios obtained with Equation 3 were used as axes in an n-dimensional space, where $n = 12$ for A ring ratios and $n = 8$ for B ring ratios. The mean location in the cluster space for the normal eye responses was determined, and the Euclidean distance (Equation 4) from this mean location to each individual response was then calculated (using a leave-one-out approach to calculate distance to normal eye responses).

$$Euclidean\ Distance = \sqrt{\sum_{i=1}^{n} (R_i - R_{HM,i})^2} \quad (4)$$

In Equation 4, R is the ratio from Equation 3, R_{HM} is the mean ratio for normal eyes (*Healthy Mean*), and i is the electrode number.

In addition, a support vector machine (SVM) approach implemented in Matlab (MathWorks, Natick, MA, USA) was used to evaluate the ability to automatically detect local lesions with meERG data. Input to the SVM was a-wave or b-wave amplitudes on all 25 electrodes, or a-wave or b-wave ratios (Equation 3). The 39 data sets (26 healthy eye responses, 13 lesion eye responses) were divided into 10 groups, 9 for training and 1 for testing (90/10 cross-validation); group membership was rotated and training repeated until every data set was in the test group at least once. The data were shuffled and the 90/10 cross-validation was repeated 20 times to obtain reliable repeated measures of true positive and true negative rates despite the modest sample size. Reported rates are the average of these 20 repeated measures.

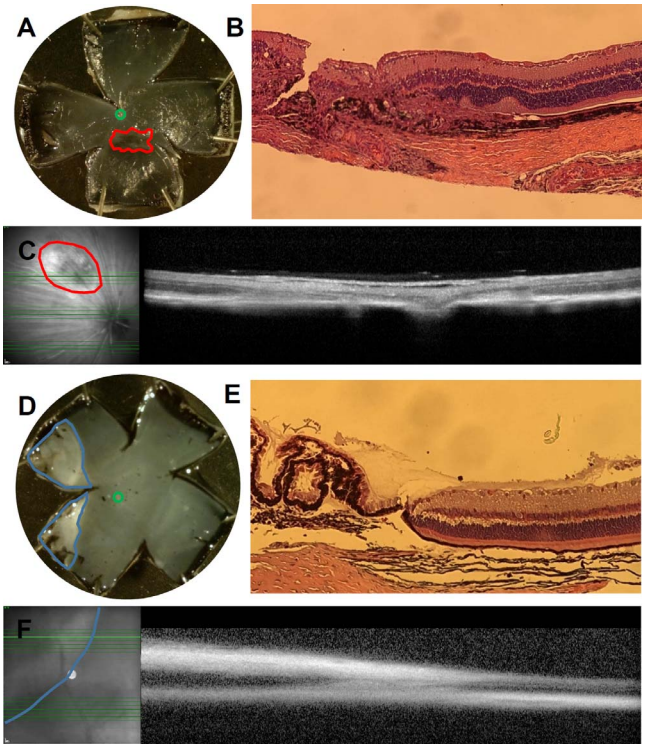

FIGURE 4. Representative experimental lesions in central and peripheral retina. (**A**) Flat-mount eye cup prepared and photographed following fixation of tissue. Lesion created by laser photocoagulation is outlined in *red* (area = 1.01 mm^2, center of lesion 1.11 mm from ONH, circled in *green*). (**B**) Histologic cross section of retina near margin of lesion shown in panel **A**. (**C**) OCT image showing one slice through a photocoagulation lesion (outlined in *red*); note significant disruption of photoreceptor layer, RPE, and Bruch's membrane. (**D**) Flat-mount preparation showing lesion created by cryocoagulation; lesion outlined in *blue* (area = 6.56 mm^2, center of lesion 2.27 mm from ONH, circled in *green*). (**E**) Histologic cross-section of retina near margin of lesion shown in panel **D**. (**F**) OCT image showing one slice through a cryocoagulation lesion (border of lesion traced in *blue*); note complete retinal detachment and swelling of the neural retina.

RESULTS

Healthy Eye meERG Responses

The meERG responses from 26 healthy eyes were evaluated for amplitude at $t = 4$ ms (leading edge of the a-wave) and at the peak of the b-wave. Each data set was interpolated to form a smooth corneal potential map (Equation 1) and then normalized by converting to standard score (Equation 2). The 26 normalized data sets were then averaged to yield the mean healthy eye response in this study, shown in Figure 3. Panels A and D show the standard score potential maps, and a slight, but not statistically significant, nasal–temporal asymmetry in the healthy eye response is suggested. Panels A and D, and all interpolated potential maps shown, are two-dimensional projections of the hemispherical cornea surface. To quantify and plot spatial asymmetry, the measured values were converted to dimensionless ratios (Equation 3) and are plotted in panels B, C for a-wave values, and panels E and F for b-wave values. The standard deviation of these ratios across animals was approximately 1.1% of the mean ratio value; ± 2 SD from the mean are plotted as dashed lines in panels B, C, E, and F.

Pretreatment normal eye responses (n = 18) were compared with posttreatment normal eye responses (i.e., repeated measures in control eyes, n = 8) to assess

Table 1. Area, Eccentricity (Measured From ONH), and Retinal Location (Relative to ONH) of Experimental Lesions

Central Lesion, Photocoagulation				Peripheral Lesion, Cryocoagulation			
Animal Number	Lesion Area, mm²	Distance From ONH, mm	Location of Lesion*	Animal Number	Lesion Area, mm²	Distance From ONH, mm	Location of Lesion*
Rat 1	1.01	1.11	I	Rat 5	3.71	2.81	T
Rat 2	2.29	1.21	IT	Rat 6	6.56	2.27	T
Rat 11	1.10	1.01	I	Rat 7	4.11	3.01	T
Rat 16	0.94	0.94	I	Rat 8	10.19	3.02	S
				Rat 9	5.95	3.20	I
				Rat 10	14.90	3.19	ST
				Rat 12	6.74	3.15	S
				Rat 13	2.77	3.40	T
				Rat 15	5.90	3.41	IT

* S, N, I, and T are superior, nasal, inferior, and temporal, respectively. Mean total retinal area = 44.10 mm² ($n = 6$).

repeatability. The mean a-wave amplitudes across the 25 meERG electrodes between pre- and posttreatment responses were significantly different (–635 ± 101 μV and –485 ± 100 μV, respectively; $P = 0.004$). The spatial distributions of a-wave potentials were not significantly different for pre- and posttreatment eyes; the distances of each response from the normal mean response (Equation 4) were 3.1 ± 0.9 and 4.4 ± 3.0, respectively ($P = 0.27$). There is no clear explanation for the significant posttreatment reduction in absolute ERG amplitudes; one possibility is stress from repeated anesthesia (three times in 1 week). The meERG-based measurements of corneal potential distribution are more repeatable than conventional absolute amplitude measures, although posttreatment potential distributions were more variable between animals.

Lesion Eye meERG Responses

The main objective of this study was to evaluate the effect of experimental lesions on meERG responses, which would begin to assess diagnostic utility of meERG recording for local areas of dysfunction. Representative flat-mount eye cups are shown in Figure 4 for eyes that received central photocoagulation and peripheral cryocoagulation lesions. The lesion area and distance from the optic nerve head for all 13 treated eyes are provided in Table 1. Photocoagulation lesions ranged from 2.1 to 5.2% of total retinal area; cryocoagulation lesions ranged from 6.3 to 33.9% of total retinal area. Also shown in Figure 4 are representative retinal cross-sections illustrating the complete loss of the organized retina and adjacent RPE within the lesion area.

The effect of the experimental lesions on the spatial distribution of corneal potentials was visualized by creating normalized potential difference maps, as illustrated in Figure 5. Potential difference maps are shown for two representative eyes (one central lesion, one peripheral lesion) in Figure 6. The spatial differences in absolute amplitudes across the cornea are still modest in eyes with lesions, with local values rarely exceeding ± 3% of the average value across all electrode positions. The effect of the experimental lesions observed via meERG recording was a change in the spatial distribution of the nearly uniform potentials, as emphasized in the normalized potential difference maps.

The asymmetry in corneal potentials was quantified using the ratio approach for each eye, using the A ring electrode values and the B ring electrode values. The resulting ratios, in red and blue in Figure 6, are plotted along with the mean ± 2 SD (approximate 95% confidence interval) for the 26 healthy eyes (in black). For multiple electrode positions, the ratios from the lesion eye response are 2 or more SD from the mean healthy eye response (i.e., outside of the "donut" bounded by the dashed lines). Note that the relatively large area of damage in the eye shown in Figure 6H resulted in a widespread reduction in a-wave and b-wave amplitudes (broad areas of slightly warmer and slightly cooler colors in the difference maps of panels I and L, respectively), causing the a-wave and b-wave amplitudes to appear relatively higher than the mean on the side of the cornea opposite of the lesion (focused areas of cooler and warmer colors at the right margins of panels I and L, and increase ratio values in panels J and M, respectively).

For lesions in peripheral retina, the local differences in corneal potential values were generally aligned with the radial

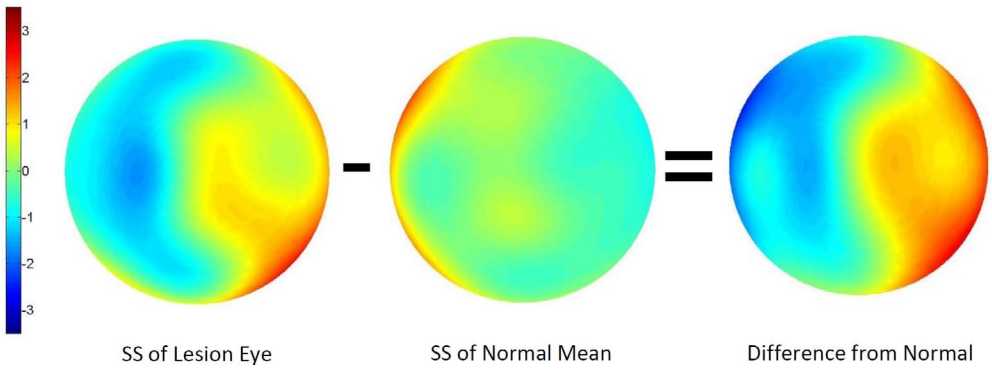

Figure 5. Deriving corneal potential maps that illustrate the difference from the normative data set. For each location on the normalized potential map, the average response of the healthy eyes (c.f. Fig. 3) was subtracted from the response of an individual. The resulting difference map plots the distance the individual response was from the normal mean, in units of standard deviations of the normative data.

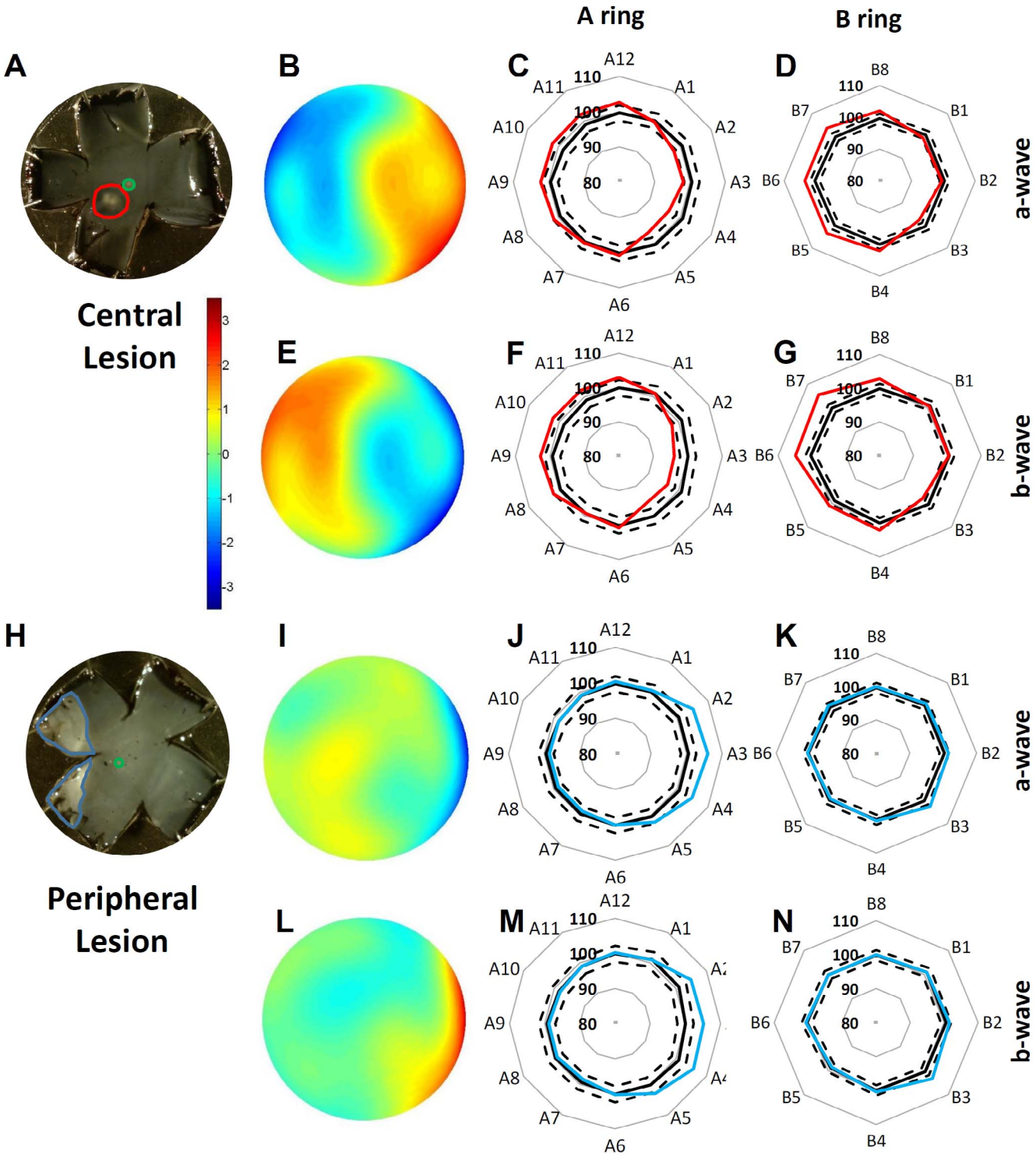

Figure 6. Representative meERG results for eyes with experimental lesions. (**A**) Flat-mount eye cup showing central lesion outlined in *red* (area = 2.29 mm^2, centered 1.21 mm from ONH, circled in *green*). (**B**) Difference map of corneal potentials plotting number of standard deviations from the average normal eye response at each location for this eye (c.f. Fig. 5). Evaluation based on meERG responses at $t = 4$ ms. Electrodes A1 and B7 not working in this experiment; amplitude values at these locations were interpolated from the remaining 23 electrode values. (**C**) A ring electrode ratios (Equation 3), showing normal eye mean ± 2 SD (*solid* and *dashed black lines*, respectively) and the ratios for this individual animal (*red line*), evaluated at $t = 4$ ms. (**D**) B ring electrode ratios, showing normal eye mean ± 2 SD (*solid* and *dashed black lines*) and the ratios for this individual animal (*red line*), evaluated at $t = 4$ ms. (**E–G**) Analysis as in panels **B** through **D**, respectively, for meERG response amplitudes evaluated at the peak of the b-wave. (**H**) Flat-mount eye cup showing peripheral lesion outlined in *blue* (area = 6.56 mm^2, centered 2.27 mm from ONH, circled in *green*). All 25 meERG channels were working in this experiment. (**I–N**) Analysis as in panels **B** through **G**, respectively, for the eye shown in panel **H**.

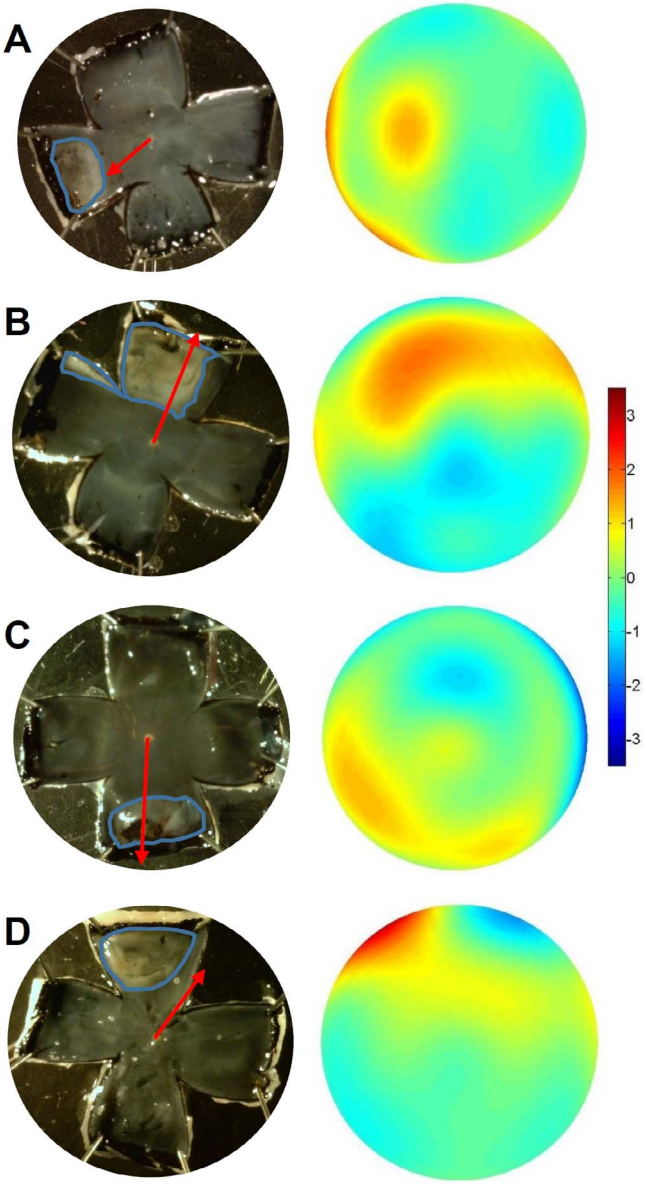

FIGURE 7. Correlation of shift in corneal a-wave potentials with location of the lesion. (**A**) Left image is the flat-mount eye cup photograph showing the cryocoagulation lesion area (outlined in *blue*). Superimposed in *red* is a vector indicating the magnitude and direction of the global shift in corneal potentials compared to the average healthy eye, vector origin at the ONH. *Right image* is the difference map of corneal potentials for the eye on the *left*. (**B–D**) Three additional eyes with peripheral lesions presented as in panel **A**.

direction of the lesion. Figure 7 shows four examples of peripheral lesion eyes, along with the corresponding potential difference maps based on a-wave amplitudes. Warmer colors indicate a reduction in amplitude from the mean healthy eye response (i.e., a less negative a-wave is a change in the positive direction), which occurs on the side of the cornea nearest the lesion.

Values for the 25 electrode locations were extracted from the potential difference maps (local standard score and radial direction relative to corneal pole) and combined to form a "shift vector" that summarized the magnitude and direction of the global shift in corneal potentials as a result of the lesion; these shift vectors are shown in red on the flat-mount photographs in Figure 7. Seven of nine eyes with peripheral lesions showed good correlation between the direction of shift in corneal potentials and the location of the lesion ($R^2 = 0.81$). The magnitude of the global shift was weakly correlated with the area of the lesion ($R^2 = 0.22$).

The global shifts in corneal potentials for the four eyes with central lesions did not appear to be correlated with the location or size of the lesion, even though three of the four eyes had measurably abnormal distributions of corneal potentials, as described in the next section.

Sensitivity to Experimental Lesions

The unique information provided by meERG recording is the relative spatial distribution of potentials over the corneal surface. This spatial distribution can be analyzed independently of the absolute amplitude of potentials. Sensitivity to the experimental lesions created here was evaluated using a cluster analysis and using a support vector machine; both approaches were used to classify measures of relative spatial distribution and absolute amplitudes.

The 12-dimensional Euclidean distances (Equation 4) based on a-wave amplitudes are plotted in the histogram of Figure 8A. As expected, the healthy eye responses (black bars) exhibit short distances from the healthy mean. The central and peripheral lesion eye responses (red and blue bars, respectively) are typically farther from the healthy mean. Grouping all lesion eyes together, a ROC curve was determined; the area under the curve was 80%. This level of sensitivity and specificity was based solely on the normalized spatial distribution of corneal potentials, in the absence of absolute amplitude information.

ROC curves for several additional analyses were determined (b-wave ratios, ratios based on the a-wave/b-wave amplitude quotient, B ring electrodes, and combined A+B ring electrodes) and are summarized in Table 2. In general, an analysis of a-wave amplitudes yielded the highest area under the curve values and was therefore most useful in detecting abnormal potential distributions for these lesions.

To compare meERG to conventional single-electrode ERG, the amplitudes recorded on the A ring electrodes were averaged to represent the single value sensed by a ring-type ERG electrode (e.g., the Burian–Allen ERG electrode). The simulated conventional a-wave amplitude values for all data sets are plotted in the histogram of Figure 8C. The area under the curve for the corresponding ROC curve, shown in panel D of Figure 8, is 84% (b-wave analysis summarized in Table 2). Sensitivity and specificity for amplitude-based conventional ERG and spatial distribution-based meERG are comparable for these lesion types.

A SVM was trained to detect abnormal responses in this data set and then evaluated for sensitivity and specificity. The input to the SVM was either the absolute amplitudes on all 25 electrodes or the ratio values for the 12 A ring electrodes. The results are summarized in Table 3, where a comparison is made with the cluster analysis results for simulated conventional ERG (i.e., average of A ring electrodes, top row), the absolute amplitude values on all 25 electrodes (second row), and the A ring electrode ratio values (third row). The best detection (D = sensitivity + specificity) was obtained using the SVM with input of absolute amplitudes on all 25 electrodes ($D = 164$), followed closely by the cluster analysis approach based on A ring ratio values of a-wave amplitudes ($D = 162$), which is independent of absolute amplitude information.

The effect of experimental lesions on the absolute amplitude of corneal potentials was greater than expected based on lesion area. The percent reduction in posttreatment a-wave amplitude (when compared with pretreatment, average

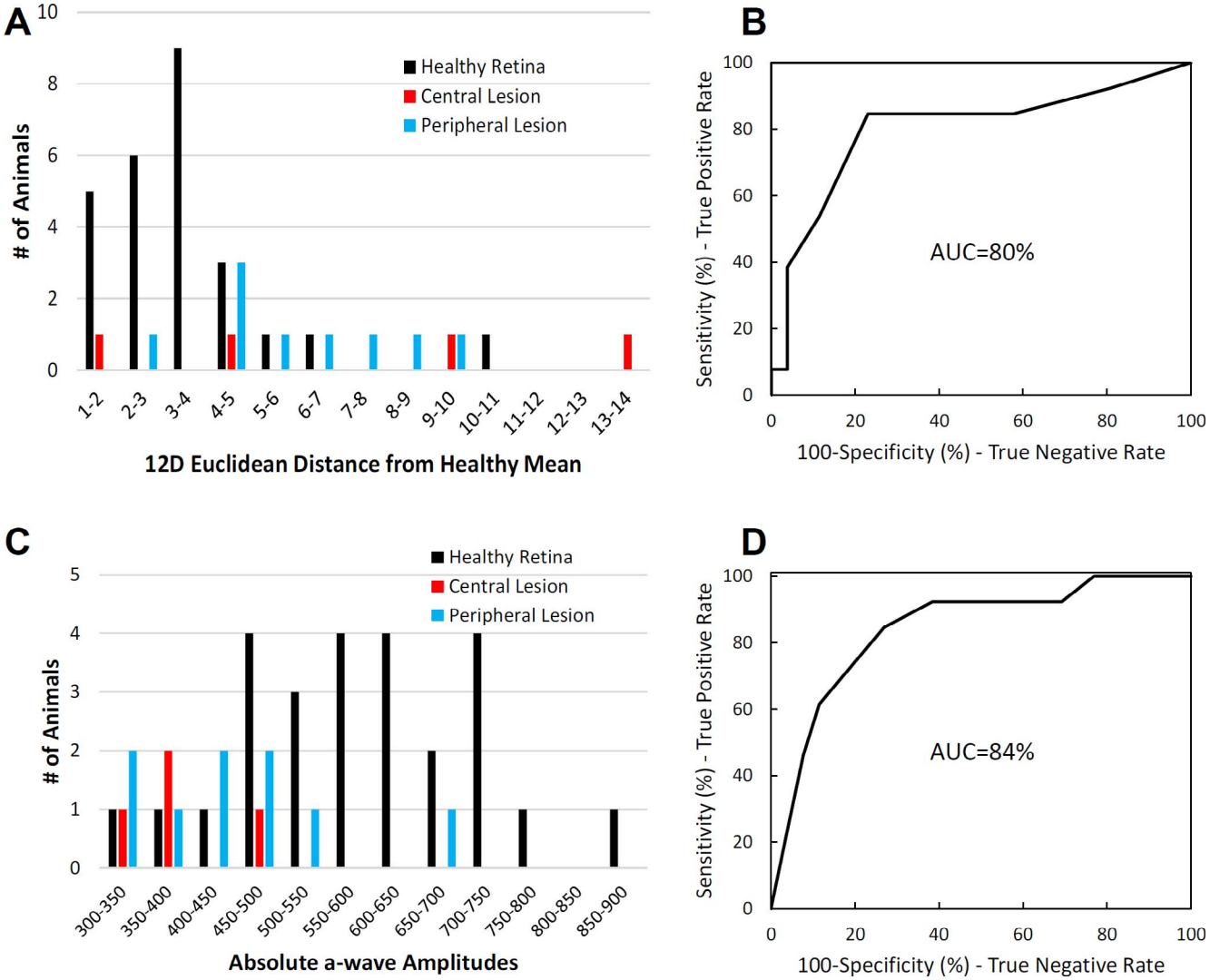

Figure 8. Sensitivity and specificity of meERG a-wave amplitudes for localized lesions. (**A**) Cluster analysis based on normalized spatial differences in corneal potentials (i.e., in the absence of absolute amplitude information). Data from 26 healthy eyes (*black*), 4 eyes with central lesions (*red*), and 9 eyes with peripheral lesions (*blue*). Euclidean distance from the healthy mean based on 12 feature values (A ring amplitude ratios, Equation 3). (**B**) ROC curve based on the histogram in panel **A**. (**C**) Cluster analysis of the same animals (colors as in **A**–**B**), using the average absolute amplitude of the corneal potentials measured on the A ring electrodes (to simulate a conventional single-channel ring electrode), evaluated at $t = 4$ ms. (**D**) The ROC curve based on the histogram in panel **C**.

value on 12 A ring electrodes) was compared to the lesion area (expressed as a percentage of retinal area) using linear regression (not shown). For peripheral lesions, the amplitude reduction was somewhat correlated with lesion area (R^2 = 0.48) and approximately 15% greater than expected based on lesion area (slope = 1.15). For central lesions, the reduction in ERG amplitude was highly correlated with lesion area (R^2 = 0.98), but approximately seven times greater than expected based on lesion area (slope = 7.35). This suggests that a reduced visual response was present for retina well beyond the area of obvious damage in the flat-mount preparations, especially for the photocoagulation model, or that tissue disruption altered the ERG current paths. For all posttreatment meERG recording, in control animals as well as animals with experimental lesions, there was an additional reduction in meERG amplitudes of approximately 12% that was independent of lesion area (*y*-intercept) attributed to the general experimental procedures (repeated anesthesia, fundus photog-

Table 2. Area Under the ROC Curve Based on Several Features Available in the meERG Response

	Area Under the Curve, %								
	a-wave			b-wave			a-wave/b-wave		
Classification Features	A ring	B ring	A+B	A ring	B ring	A+B	A ring	B ring	A+B
Spatial ratios	80	81.5	80.9	78.9	68.6	79.1	65.9	67.7	74.4
Simulated conventional ERG	84.1			80.9			31.2		

Table 3. Sensitivity and Specificity to Local Experimental Lesions for Conventional ERG and for meERG Using Cluster Analysis and Support Vector Machine Classification

	a-wave		b-wave	
Classification Features	**Sensitivity, %**	**Specificity, %**	**Sensitivity, %**	**Specificity, %**
Simulated conventional ERG				
A ring average	85	73	92	50
meERG cluster analysis				
Absolute amplitudes on 25 electrodes	85	46	80	65
A ring ratios	85	77	85	62
meERG SVM				
Abs. amp. 25 electrodes	73	84	72	92
A ring ratios	79	52	74	30

raphy, and meERG recording within 6–7 days) and short recovery time between photocoagulation and cryocoagulation treatments and posttreatment meERG recording.

Discussion

The meERG approach yields a complete spatial map of corneal potentials for every time point in the flash ERG response; this is a form of ERG data that has not previously been accessible. The use of multi-electrode recording allows spatial information to be obtained using relatively simple full-field flash stimuli.

It should be noted that meERG recording technology is amenable to all full-field flash ERG protocols and provides all of the information of conventional single-electrode ERG recording (amplitude and kinetics) in addition to the unique spatial information. Analysis based on a-wave amplitudes was effective for detecting the experimental lesions employed here; other flash ERG response parameters (e.g., photopic negative response amplitude or oscillatory potential amplitude) may be more appropriate for other types of retinal insult (glaucoma or vascular disease, respectively).

Earlier efforts to record and analyze ocular surface potential maps concluded that the spatial distribution of corneal potentials is influenced by the spatial distribution of the current sources, that is, the distribution of activity in the retina; this was demonstrated empirically with experimental photocoagulation lesions[4,5] and theoretically predicted using models of local areas of deficit.[7,8]

It is difficult to compare the present results to earlier empirical work because of the use of different species (rabbit, dog), experimental setups (isolated perfused eye), incomplete description of the experimental lesions, and different recording locations (limbus, sclera). However, the earlier empirical work, and the ERG electric field models developed by Job et al.[8] all agree that ocular surface potentials decrease in locations near the site of experimental lesions in the retina. The present study confirms this finding using comprehensive corneal potential maps, each derived from the response to a single full-field flash, representing a technical solution with the potential for clinical application.

The value of corneal potential maps depends largely on the ability to interpret them with regard to spatial differences in retinal function. The data presented here demonstrate that the normalized potential maps for healthy eyes are quite consistent and that measurable differences from the normal spatial distribution are created by experimental lesions. This is true for lesions in the central retina and lesions in the far-peripheral retina, where very few clinical tests are effective.

The lesion models used in this study resulted in complete disruption of the neural retina in the targeted area, but also damaged the RPE and Bruch's membrane. At the time of the posttreatment meERG recording (2 to 3 days after lesion creation), local retinal detachment, subretinal bleeding, and swelling of the retina surrounding the area of obvious retinal damage were observed in some animals (OCT imaging, not shown). These alterations to the retina and adjacent tissues resulted in a reduced retinal response (probably beyond the area of obvious damage) and, importantly, altered current paths underlying the ERG. The outer limiting membrane, and the combined RPE and Bruch's membrane, form high-resistance layers that play a critical role in shaping the ERG[17,18]; disrupting these layers creates a current shunt at the location of the lesion, reducing the currents (and voltages) at the cornea and extraocular tissues. These observations likely explain some of the posttreatment reductions in ERG potentials, which were greater than expected based on the percent of the retina occupied by the lesions (most notable for central photocoagulation lesions). In addition, the poor correlation between the lesion area and magnitude of the shift in corneal potentials could also be explained by local, variable, transretinal current shunts. Detailed histologic information for the lesions in the present study was not available. A more complete treatment of this issue will require more complete information regarding the effects of the cryocoagulation and photocoagulation procedures and appropriate computational models.

The preliminary effort to quantitatively correlate the changes in corneal potential distribution with the location of peripheral lesions was encouraging. Future use of a species with larger eyes would facilitate evaluating lesions of smaller relative size and provide greater control over location of photocoagulation lesions. To firmly establish the sensitivity of meERG for local lesion detection in clinical applications, lesion models that closely resemble the target pathologies (e.g., localized photoreceptor loss associated with retinitis pigmentosa) will be required. The resolution of meERG recording, in terms of degree and extent of retinal dysfunction that can be measured, remains to be established. However, the simplicity and pan-retinal response of full-field flash meERG represent potential advantages over the multifocal ERG, especially for damage in the mid- and far-peripheral retina.

The ultimate goal of meERG development is to use the corneal potential maps to derive retinal activity maps through computational models. Earlier efforts to solve for location and magnitude of retinal current sources from measured surface potentials were limited by the level of anatomical detail that could be practically incorporated into the model and a lack of suitable data with which the model could be optimized and

Investigative Ophthalmology & Visual Science

validated.[7,8,19] The data presented here address the latter in a significant way.

Acknowledgments

The authors would like to thank Sarita Despande, Samuel Dreyer, and Meagan Ouy for their assistance in carrying out the meERG experiments and with the analysis of data.

Supported by bridge funding provided by the Colleges of Engineering and Medicine at the University of Illinois at Chicago.

Disclosure: **Z. Derafshi**, None; **B.E. Kunzer**, None; **E.M. Mugler**, None; **N. Rokhmanova**, None; **D.-W. Park**, None; **H. Tajalli**, None; **K. Shetty**, None; **Z. Ma**, None; **J.C. Williams**, None; **J.R. Hetling**, RetMap, Inc. (S), P

References

1. Parvaresh MM, Ghiasian L, Ghasemi Falavarjani K, Soltan Sanjari M, Sadighi N. Normal values of standard full field electroretinography in an Iranian population. *J Ophthalmic Vis Res*. 2009;4:97–101.
2. Sutter EE, Tran D. The field topography of ERG components in man—I. The photopic luminance response. *Vision Res*. 1992; 32:433–446.
3. Hood DC, Bach M, Brigell M, et al. ISCEV standard for clinical multifocal electroretinography (mfERG) (2011 edition). *Doc Ophthalmol*. 2012;124:1–13.
4. Holland MG, Herr N. The electroretinographic potential field. Localization of retinal lesions. *Am J Ophthalmol*. 1964;57: 639–645.
5. Cringle SJ, Alder VA. The effect of a retinal lesion on the distribution of B wave potentials on the sclera. *Curr Eye Res*. 1987;6:1109–1114.
6. Krakova Y, Tajalli H, Thongpang S, et al. Spatial differences in corneal electroretinogram potentials measured in rat with a contact lens electrode array. *Doc Ophthalmol*. 2014;129:151–166.
7. Davey KR, Thompson B, Wang SM, Koblasz A, Nation B. Predicting distributed retinal source activity from ERG data—Part I: field theoretic approach. *IEEE Trans Biomed Eng*. 1988;35:942–947.
8. Job HM, Keating D, Evans AL, Parks S. Three-dimensional electromagnetic model of the human eye: advances towards the optimization of electroretinographic signal detection. *Med Biol Eng Comput*. 1999;37:710–719.
9. He B, Wu D. Laplacian electrocardiography. *Crit Rev Biomed Eng*. 1999;27:285–338.
10. He B, Lian J. High-resolution spatio-temporal functional neuroimaging of brain activity. *Crit Rev Biomed Eng*. 2002; 30:283–306.
11. Ciulla TA, Criswell MH, Danis RP, Williams JI, McLane MP, Holroyd KJ. Squalamine lactate reduces choroidal neovascularization in a laser-injury model in the rat. *Retina*. 2003;23: 808–814.
12. Chu Y, Alder VA, Humphrey MF, Constable IJ. Localization of IgG in the normal and dystrophic rat retina after laser lesions. *Aust N Z J Ophthalmol*. 1999;27:117–125.
13. Humphrey MF, Chu Y, Mann K, Rakoczy P. Retinal GFAP and bFGF expression after multiple argon laser photocoagulation injuries assessed by both immunoreactivity and mRNA levels. *Exp Eye Res*. 1997;64:361–369.
14. Hu W, Criswell MH, Fong SL, et al. Differences in the temporal expression of regulatory growth factors during choroidal neovascular development. *Exp Eye Res*. 2009;88:79–91.
15. Suomalainen VP. Comparison of retinal lesions produced by transscleral krypton laser photocoagulation, transpupillar krypton laser photocoagulation and cryocoagulation. *Acta Ophthalmol*. 1993;71:224–229.
16. Law SK, Nunez PL, Wijesinghe RS. High-resolution EEG using spline generated surface Laplacian on spherical and ellipsoidal surfaces. *IEEE Trans Biomed Eng*. 1993;40:145–153.
17. Brindley GS. The passive electrical properties of the frog's retina, choroid and sclera for radial fields and currents. *J Physiol*. 1956;134:339–352.
18. Karwoski CJ, Xu X, Yu H. Current-source density analysis of the electroretinogram of the frog: methodological issues and origin of components. *J Opt Soc Am*. 1996;13:549–556.
19. Krakau CET. On the potential field of the rabbit electroretinogram. *Acta Ophthalmol*. 1958;36:183–207.

Investigative Ophthalmology & Visual Science